ACS SENSORS

pubs.acs.org/acssensors

Article

Protein Discrimination Using a Fluorescence-Based Sensor Array of Thiacarbocyanine-GUMBOS

Rocío L. Pérez, Mingyan Cong, Stephanie R. Vaughan, Caitlan E. Ayala, Waduge Indika S. Galpothdeniya, John K. Mathaga, and Isiah M. Warner*

Cite This: *ACS Sens.* 2020, 5, 2422–2429

Read Online

ACCESS | Metrics & More | Article Recommendations | Supporting Information

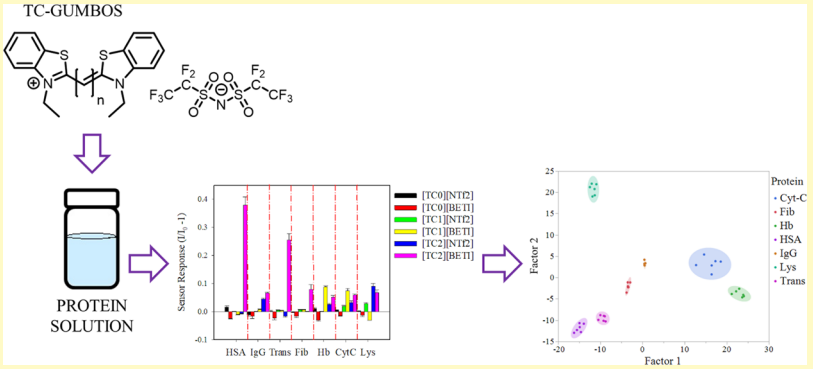

ABSTRACT: Sensitive and selective detection of proteins from complex samples has gained substantial interest within the scientific community. Early and precise detection of key proteins plays an important role in potential clinical diagnosis, treatment of different diseases, and proteomic research. In the study reported here, six different compounds belonging to a group of uniform materials based on organic salts (GUMBOS) have been synthesized using three thiacarbocyanine (TC) dyes and employed as fluorescent sensors. Fluorescence properties of micro- and nanoaggregates of these TC-based GUMBOS formed in phosphate buffer solutions are studied in the absence and presence of seven proteins. Fluorescence response patterns of these TC-based GUMBOS were analyzed by linear discriminant analysis (LDA). The constructed LDA model allowed discrimination of these seven proteins at various concentrations with 100% accuracy. The sensing and discrimination abilities of these TC-based GUMBOS were further evaluated in mixtures of two major proteins, i.e., human serum albumin and hemoglobin. Fluorescence response patterns of these mixtures were analyzed by LDA. This model allowed discrimination of various mixtures with 100% accuracy. Moreover, spiked urine samples were prepared and the responses of these sensors were collected and analyzed by LDA. Remarkably, discrimination of these seven proteins was also achieved with 100% accuracy.

KEYWORDS: *protein discrimination, cross-reactive sensor array, GUMBOS, linear discriminant analysis (LDA), protein mixture, real samples*

Sensitive and precise sensing of multiple proteins simultaneously is of great interest for clinical diagnosis, treatment of disease, and proteomic research.[1] Currently, the most commonly used technique for protein detection is enzyme-linked immunosorbent assay (ELISA)[2] due to its excellent specificity and sensitivity as a result of specific binding interactions between each antibody and its target protein.[3] However, high cost and poor stability of antibodies limit application of this approach for protein sensing. Other types of methodologies include polyacrylamide gel electrophoresis coupled to mass spectroscopy (see ref 4 for example and ref 5 for electrochemical methods). The problem is that these techniques are time-consuming, requiring complicated synthetic procedures, expensive, and sometimes not capable of resolving complex mixtures of proteins. As alternatives, cross-reactive sensor arrays, known as electronic noses (e-noses), have been employed for high-throughput detection and discrimination of proteins.[6] In this regard, diverse sensor systems have been applied for array sensing of proteins, including functionalized gold nanoparticles,[6a,7] fluorescent polymers,[6b,8] carbon nanotubes,[7c,9] and porphyrins.[10] Among these sensing materials, the use of fluorescence as a detection technique is the method of choice due to its high sensitivity.

Received: March 11, 2020
Accepted: July 20, 2020
Published: July 20, 2020

https://dx.doi.org/10.1021/acssensors.0c00484
ACS Sens. 2020, 5, 2422–2429

However, broad application of this approach is hindered by complicated design and syntheses.

In this study, a fluorescence-based sensor array using a group of uniform materials based on organic salts (GUMBOS) for sensitive and accurate protein discrimination is developed. The concept of GUMBOS has been introduced by our research group in 2008 as solid-phase organic salts with tunable properties similar to ionic liquids (ILs) but with a wider range of melting points (25−250 °C) than ILs (melting point, <100 °C).[11] GUMBOS employed in the study reported here consist of a series of three fluorescent thiacarbocyanine (TC) cations bearing different methine chain lengths. TC dyes belong to a dye family called polymethine dyes (PD), where their alternating π-electrons along the methine chain produce high polarizability, which provides strong attractive forces between molecules.[12] Thus, the structures of TC dyes allow extended and stable aggregation.[13]

It has been found that aggregation of PD highly depends on the surrounding environment composition.[14] In particular, noncovalent interactions between cyanine dyes and biomolecules are of considerable interest[14a,i,15] within the scientific community. These interactions modify the aggregation of dyes and hence remarkably alter their photophysical and photochemical properties. Due to the favorable properties of TC dyes noted above, these compounds may have considerable potential for use in fluorescence protein sensing. In this study, bis(trifluoromethylsulfonyl)imide ([NTf2]−) and bis[(pentafluoroethyl)sulfonyl]imide ([BETI]−) anions were used to increase the hydrophobicity of GUMBOS and facilitate aggregation at low concentrations.

The six TC-based GUMBOS-based sensors employed in this sensor array exhibit varying degrees of aggregation when mixed with seven proteins, thus providing distinct fluorescence responses. These resulting responses exhibit cross-reactive patterns, which can be statistically analyzed to discriminate proteins at diverse concentrations. The fluorescence sensor array developed in this study shows great potential for highly sensitive diagnostic applications.

RESULT AND DISCUSSION

Characterization of TC-GUMBOS Sensors. The chemical structures of TC-GUMBOS used in this study are shown in Figure 1. Formation of TC-GUMBOS was confirmed by ESI

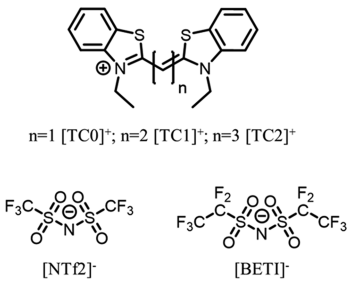

Figure 1. Chemical structures of synthetized TC-GUMBOS.

spectroscopy (Figures S1−S6) as well as FT-IR spectra (Figures S7−S9). Analysis in positive ion mode (Figures S1A−S6A) shows the presence of intense peaks with m/z values of 339.0990, 365.1100, and 391.1300 and thus corroborated the presence of [TC0]+, [TC1]+, and [TC2]+ cations, respectively (Table S1). In the same manner, the presence of peaks with 279.92 and 379.91 m/z in negative ion mode (Figures S1B−S6B) corroborates the presence of [NTf2]− and [BETI]− anions, respectively. Product formation was also confirmed. Peaks in FT-IR spectra corresponding to both parent compounds were observed in the product spectra (Figures S7−S9).

Relative hydrophobicities of all TC-GUMBOS employed in this study were estimated using an octanol/water partition coefficient (KO/W) to evaluate their capacity to form nanostructures or aggregates in aqueous solutions. Logarithms of KO/W are listed in Table S1. As inferred by these log KO/W values, hydrophobicities of these TC-GUMBOS increase in the following order: [TC2][NTf2] < [TC1][NTf2] < [TC1][BETI] < [TC2][BETI] < [TC0][NTf2] < [TC0][BETI].

Aggregates of our TC-GUMBOS were prepared as described in Synthesis and Characterization of TC-GUMBOS and Aggregates. Analysis of TEM images presented in Figure 2

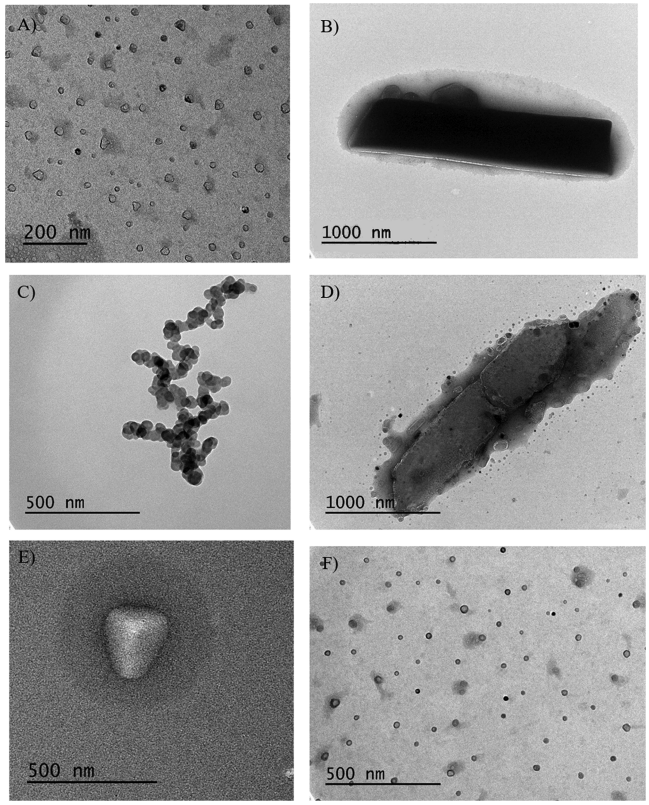

Figure 2. TEM micrograph of TC-GUMBOS aggregates: (A) [TC0][NTf2], (B) [TC0][BETI], (C) [TC1][NTf2], (D) [TC1][BETI], (E) [TC2][NTf2], and (F) [TC2][BETI].

showed that [TC0][NTf2] aggregates were composed of circular nanoparticles with sizes around (25 ± 6) nm and [TC0][BETI] aggregates were composed of rodlike morphologies (1.4 ± 0.3) × (0.17 ± 0.09) μm. Evaluation of TEM images corresponding to [TC1][NTf2] GUMBOS revealed aggregates with spherical morphology. However, their sizes were not accurately measured due to blurred edges. [TC1][BETI] GUMBOS presented rodlike shapes with average sizes of (1.2 ± 0.5) × (0.21 ± 0.08) μm. In the case of [TC2][NTf2], predominantly triangular morphologies were displayed with an average size of (200 ± 10) × (177 ± 80) nm. Last, for [TC2][BETI], spherical morphologies were obtained with average sizes of (63 ± 8) nm.

https://dx.doi.org/10.1021/acssensors.0c00484
ACS Sens. 2020, 5, 2422−2429

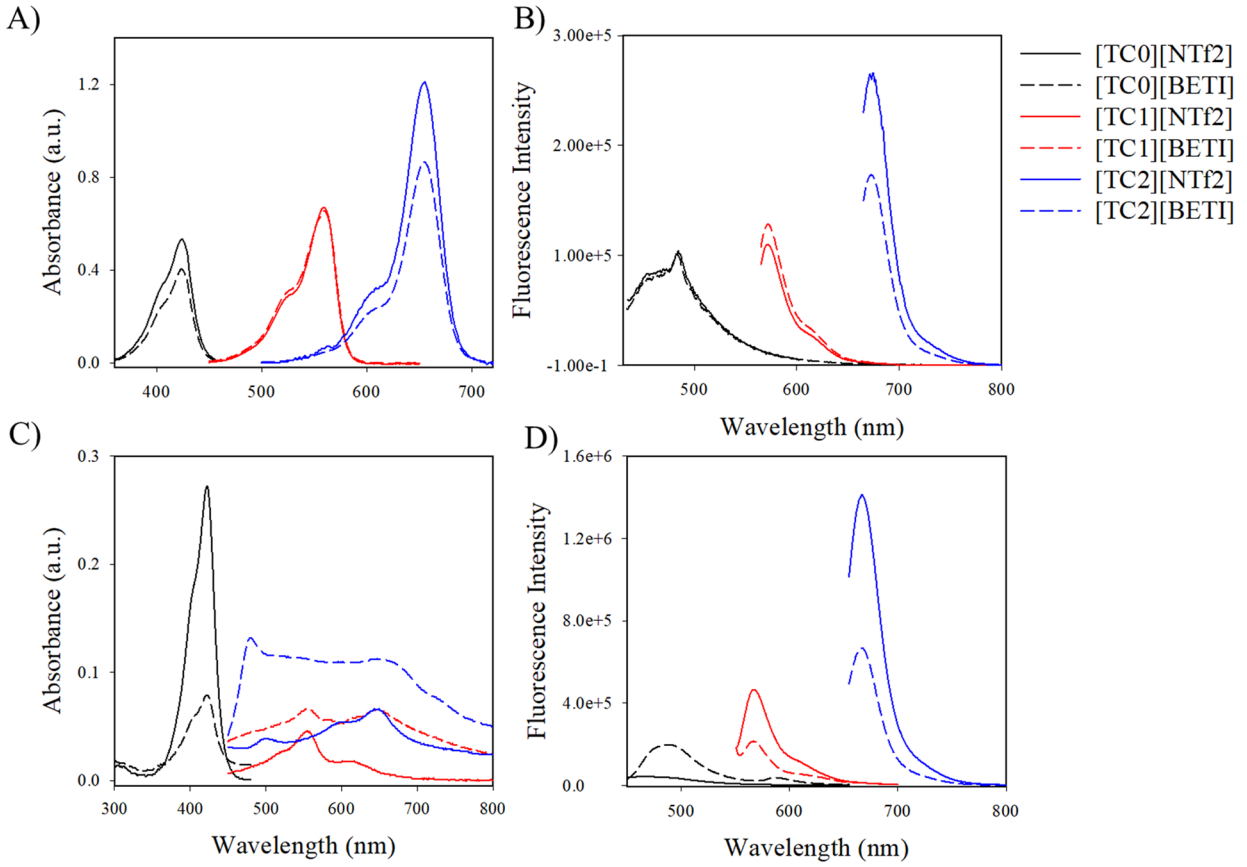

Figure 3. (A) UV−Vis and (B) fluorescence spectra of TC-GUMBOS in ethanol. (C) UV−Vis and (D) fluorescence spectra of TC-GUMBOS suspended in phosphate buffer via the reprecipitation method at a concentration of 5 μM.

Spectral Properties of TC-Based GUMBOS. Anions [NTf2]− and [BETI]− do not absorb light at wavelengths longer than 210 nm. As a result, these anions are non-fluorescent. For this reason, spectral properties of these TC-GUMBOS are completely attributed to TC cations used in the formation of these compounds. As a result of being highly hydrophobic, absorption and emission spectra for all six TC-GUMBOS were recorded at a concentration of 5 μM in ethanol. From results depicted in Figure 3A, we observed maximum absorbance wavelengths for [TC0]+, [TC1]+, and [TC2]+ as 424, 555, and 655 nm, respectively. Upon anion variation, no changes in absorption maxima were observed. Instead, a change in molar absorptivity was observed. Figure 3B displays the fluorescence emission spectra of GUMBOS when excited at their corresponding absorption maximum. Emission maxima observed for [TC0]+, [TC1]+, and [TC2]+ were at 483, 572, and 672 nm, respectively (Figure 3B).

The absorbance and fluorescence spectra of TC-GUMBOS aggregates were also evaluated in phosphate buffer (pH = 7.4). The resulting spectra are displayed in Figure 3C,D, respectively. In comparison with their ethanolic solutions, [TC0]-GUMBOS dispersions exhibit the same absorption maxima at 424 nm with relatively higher shoulders at 402 nm attributed to H-aggregation (Figure 3C). The absorption spectra for [TC1][NTf2] and [TC1][BETI] buffer dispersions show additional peaks at 615 and 650 nm, respectively, representative of J-aggregation (Figure 3C). Conversely, in the cases of [TC2][NTf2] and [TC2][BETI], the absorption spectra of these aggregates exhibit blue-shifted peaks centered at higher energy and are also attributed to H-aggregation (Figure 3C). Buffer dispersions of TC0-GUMBOS, TC1-GUMBOS, and TC2-GUMBOS were excited at 423, 541, and 645 nm, respectively, showing emission maxima at 476, 488, 565, and 665 nm for [TC0][NTf2], [TC0][BETI], TC1-GUMBOS, and TC2-GUMBOS, respectively.

Detection and Discrimination of Proteins through a TC-GUMBOS Sensor Array. Seven proteins with diverse molecular weights (MW), with and without a cofactor, and different isoelectric points (pI) were selected as sensing targets (Table S2). Among the seven selected proteins, HSA, IgG, Trans, and Fib are top four in abundant proteins of human serum.[6a] The remaining three proteins, i.e., Hb, Cyt-c, and Lys, are nonserum proteins.

In order to investigate if TC-GUMBOS dispersions were capable of discriminating between these proteins, fluorescence responses of these sensors were investigated in the presence of each protein. All fluorescence spectra were analyzed using individual protein concentrations of 0.5 g/mL, and noticeable changes in emission intensity of each TC-GUMBOS were observed. For this reason, eq 1 was employed to calculate sensor response. Figure 4A is the representation of the TC-GUMBOS sensor responses in the presence of different proteins. As shown in Figure 4A, the presence of each protein produced a varied fluorescence response with the same sensor. Additionally, in the presence of the same protein, different fluorescence responses were obtained for each TC-GUMBOS sensor. These distinct response patterns suggest feasibility of protein discrimination using these responses to build a sensor array.

https://dx.doi.org/10.1021/acssensors.0c00484
ACS Sens. 2020, 5, 2422−2429

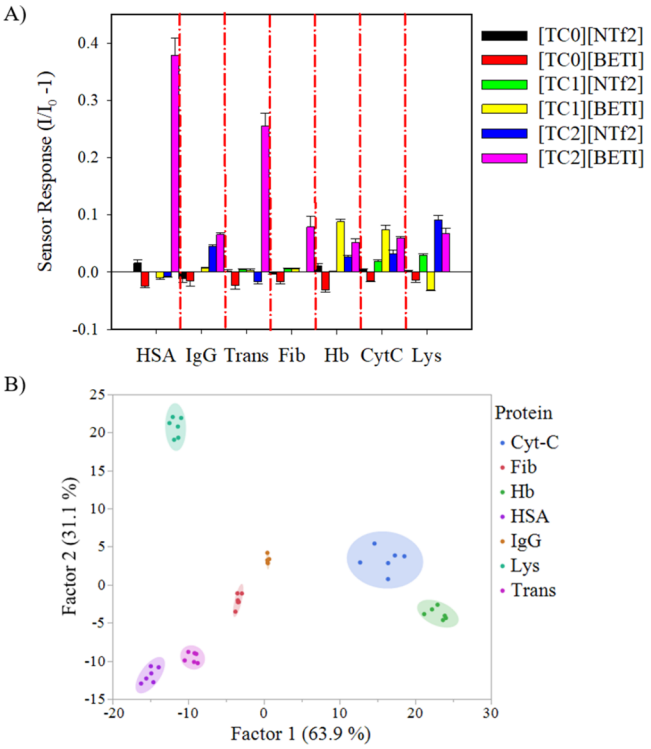

Figure 4. (A) Response of sensor array-based TC-GUMBOS for seven proteins at 0.5 μg/mL in pH 7.4 phosphate buffer. Error bars represent standard deviations of six replicate samples. Dot−dash red lines represent separate responses of each protein. (B) Canonical score plot for response patterns as obtained from LDA for seven proteins at 0.5 μg/mL. Ellipses represent 95% confidence.

In order to further validate the ability of this sensor array to discriminate proteins, the pattern responses were then subjected to multivariate statistical analyses, specifically, principal component analysis (PCA) and linear discriminant analysis (LDA). Both PCA and LDA are statistical techniques commonly used for dimensionality reduction. PCA is "unsupervised", as it ignores class labels, while LDA is a "supervised" technique and computes the linear discrimination factors that maximize the separation between multiple classes.[16]

Initially, raw data collected for the six TC-GUMBOS sensors was employed to build a predictive model with LDA. Figure 4B is a display of a two-dimensional plot of the canonical scores obtained using the entire data collected, where different proteins are well clustered in individual groups with a classification accuracy of 100%. For comparative purposes, the raw data was first processed with PCA to reduce dimensionality. Then, the first two principal components that accounted for 69.4% of variability within the data were employed to build a predictive model with LDA. This new LDA model discriminated the proteins into separate groups with an accuracy of 97.62%. In this case, one Cyt-C sample was misclassified as Hb (Figure S10). For this reason, the following statistical analysis was performed using the raw data.[17] Sensor responses and score values for the canonical factors for each replicate of the seven studied proteins are depicted in Tables S4 and S5, respectively.

Additionally, lower protein concentrations were tested to evaluate the ability of this sensor array to discriminate proteins at trace levels. Tables S6 and S7 provide the sensor response values of each protein and scores of canonical factors 1 and 2, respectively. Sensor responses obtained for these proteins at 0.1 μg/mL were analyzed by LDA. As shown in Figure S10A, relative deviations of sensor responses become larger at this concentration as expected. Figure S11B depicts successful clustering of most of the studied proteins into groups, with a clear overlap between the confidence ellipses of Hb and Cyt-C. This may be due to the presence of the heme-group in both proteins. Remarkably, the accuracy of this model at 0.1 μg/mL concentration is 100%, proving that this sensor array allows detection and discrimination of the studied proteins at low concentrations.

Moreover, the sensor response with respect to protein concentration was evaluated. Different protein concentrations (0.1−20 μg/mL) were tested using these TC-GUMBOS sensors (Figure S12). Evaluation of these results demonstrated that [TC1][NTf2] and [TC2][BETI] exhibited an increase in fluorescence intensity, resulting in positive sensor responses (eq 1) toward all seven proteins. In contrast, [TC0][NTf2] exhibited fluorescence quenching that is reflected in negative sensor responses toward IgG; [TC0][BETI] showed quenching of its fluorescence toward all seven proteins. Moreover, [TC1][BETI] presented negative sensor responses toward HSA and Lys; [TC2][NTf2] showed negative responses toward HSA and Trans. These features remained consistent over a protein concentration range of 0.1−20 μg/mL and, as anticipated, were enhanced at higher concentrations. As illustrated in Figure S13, nine concentrations were tested and grouped into nine isolated clusters in LDA plots for each protein. Discriminant accuracies were calculated to be 100% for all proteins. Since the first discriminant canonical factor (factor 1) produced greater than 99% variance, it was plotted against each protein concentration. An excellent linear relationship between canonical 1 and protein concentrations was observed, as illustrated in Figure S13. These results demonstrate that interactions between the TC-GUMBOS sensors and each protein are homogeneous and stable.

Discrimination of Mixtures of Proteins. The capacity of these TC-GUMBOS to discriminate proteins present in a mixture was also studied. For this purpose, sensor responses for mixtures of HSA and Hb with different weight ratios (100% HSA, 80% HSA + 20% Hb, 60% HSA + 40% Hb, 40% HSA + 60% Hb, 20% HSA + 80% Hb, and 100% Hb) were collected. The total protein concentration was maintained at 5 μg/mL. The raw data was employed to build a new LDA model (Table S8). As illustrated in the LDA plot (Figure 5), HSA and Hb mixtures with various ratios were well discriminated with a discriminant accuracy of 100%. Score values of canonical factors 1 and 2 are displayed in Table S9. Based on evaluation of the LDA discrimination plot displayed in Figure 5, a notable trend from 100% HSA samples with higher scores to 100% Hb samples with lower values of canonical scores was observed. However, an exemption for the mixture of 80% HSA−20% Hb samples that was presented with the lowest canonical score values was observed. In order to understand why these samples are outside this trend, a hierarchical cluster analysis (HCA) was performed (Figure S14). Evaluation of the HCA plot demonstrated that all samples are separated and are distributed into three different clusters. One of those clusters included 80% HSA−20% Hb samples, indicating that these samples are less related to the other samples.

Protein Discrimination in Real Samples. Additionally, to explore application of this sensor array to more complex,

https://dx.doi.org/10.1021/acssensors.0c00484
ACS Sens. 2020, 5, 2422−2429

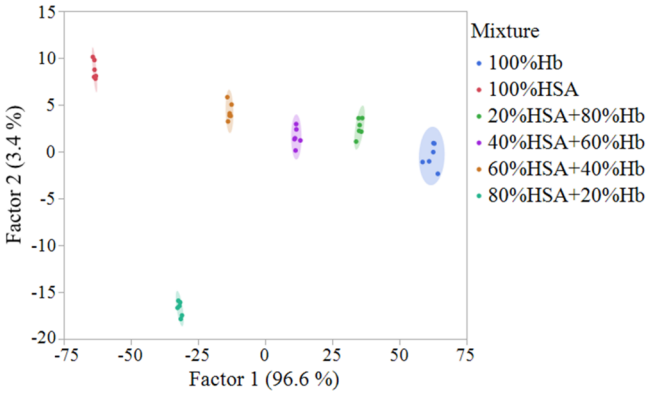

Figure 5. Canonical score plot for discrimination of HSA, Hb, and mixtures at 5 μg/mL. Ellipses represent 95% confidence.

real samples, artificial urine that contains various organic and inorganic salts was used as media for discrimination of the seven studied proteins at 5 μg/mL. Sensor response values and scores of canonical factors 1 and 2 are presented in Tables S10 and S11, respectively. Figure 6 is a representation of a two-

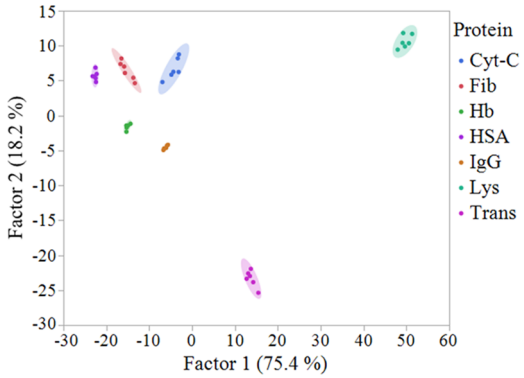

Figure 6. Canonical score plot for discrimination of all seven proteins in artificial urine

dimensional canonical score plot. Evaluation of this plot indicates that this sensor array is suitable for discrimination of these seven proteins in a urine sample, providing seven different clusters without overlap. Discriminant accuracy was calculated to be 100%, demonstrating the high feasibility of this fluorescence sensor array to discriminate proteins in real samples at low concentrations.

Discussion of the Possible Sensing Mechanism. Spectral properties of PD are highly dependent on the surrounding media.[18] In recent decades, studies of noncovalent interactions between PD and biomolecules are of considerable interest.[15a,19] We hypothesize that noncovalent interactions occur in the sensing process between TC-GUMBOS and proteins studied, which results in variation of aggregation, rotational/stretching motion, etc. Among these effects, we believe that the formation of different types of aggregates is the major driving force for emission changes. The absorption and emission spectra of these six sensor elements with different proteins are depicted in Figure S15. It is well established that thiacarbocyanine dyes could form H-aggregates that cause nonradiative decay, thus leading to decreased emission,[20] and as J-aggregates that cause increased emission.[19a] As an example, the [TC2][BETI] sensor element exhibited positive responses toward all seven proteins. As observed in Figure S15F, in the presence of proteins, the intensity of H-aggregation absorption at 476 nm decreased and the monomer absorption peak at 655 nm was amplified. This behavior indicates that [TC2][BETI] nanoGUMBOS are dissociating into monomers in the presence of proteins. As a result, the fluorescence spectra (Figure S15F) exhibited increased fluorescence emission of [TC2][BETI] as proteins were introduced into the system. Conversely, fluorescence emission of [TC0][BETI] decreased as proteins were incorporated (Figure S15B). These changes are attributed to the formation of H-aggregates in the presence of proteins, which is verified using absorption spectra as shown in Figure S15B, where blue-shifted peaks were observed as proteins were introduced. In addition, H-aggregates exhibit a red shift of the emission spectrum and remarkably lower fluorescence intensity (Figure S15B).

[TC1][NTf2] and [TC2][BETI] nanoGUMBOS showed positive responses toward all seven proteins; however, this phenomenon cannot be explained using formation of J-aggregates in the presence of proteins. Analysis of absorption spectra (Figure S15C) indicates that [TC1][NTf2] does not form H-aggregates. Instead, a red-shifted peak was observed at 610 nm, which is attributed to absorption of J-aggregates. In the presence of proteins, the absorption peaks of the monomer at 555 nm and the shoulder peak of J-aggregates increased. This effect is more difficult to distinguish in [TC2][BETI] absorption spectra (Figure S15 F). However, emission spectra confirmed formation of J-aggregates with a slightly red-shifted emission peak at 638 nm. Interestingly, emission intensity of the monomer also increased with addition of proteins. Moreover, it has been reported in the literature that TC1 dyes form J-aggregates in the presence of HSA, corroborating the results obtained in this work.[15a] This is probably due to formation of a dye monomer−protein complex, which would restrict intramolecular rotational motion. The intramolecular rotational motions of the flexible polymethine chain in TC dyes would lead to rapid nonradiative decay.[15a,19a,21] As a result, noncovalent interactions (e.g., hydrogen bonding, hydrophobic interaction, and electrostatic attraction) with proteins are very likely to stabilize TC dyes, thus restricting the nonradiative decay caused by rotation and twist and hence increasing the quantum yield of these TC dyes.[22] Therefore, we hypothesize that the slightly red-shifted monomer absorption peak (Figure S14C) is also due to noncovalent interactions between the dye monomer and protein.

In the case of [TC0][NTf2], [TC1][BETI], and [TC2]-[NTf2], responses in the presence of proteins were mixed (Figure S15A,D,E, respectively). This behavior could be explained via specific H- or J-aggregation of the nano-GUMBOS with specific proteins. In our group, it has been proven that some cyanine-based nanoGUMBOS form H- and J-aggregates within the nanoparticles.[23] In this work, a similar mechanism may be apparent. Moreover, it has been shown that certain cyanine dyes form either J- or H-aggregates in the presence of different types of biomolecules.[24] We believe that an increase in fluorescence emission intensity here is due to J-aggregate components in nanoGUMBOS, which are more prevalent than H-aggregates. Conversely, a decrease in fluorescence emission intensity occurs when H-aggregates were predominant in the nanoparticles.

https://dx.doi.org/10.1021/acssensors.0c00484
ACS Sens. 2020, 5, 2422−2429

CONCLUSIONS

In this study, we have developed a rapid and effective fluorescence sensor array for protein discrimination. This sensor array was constructed using a series of TC-GUMBOS, which were easily synthesized through a simple ion metathesis reaction. The variation of TC-GUMBOS aggregation due to noncovalent interaction with proteins was believed to be the major driving force for fluorescence protein sensing. Other noncovalent interactions also play indispensable roles, e.g., molecular rotation restriction. It has been successfully demonstrated that this sensor array is capable of discriminating proteins at concentrations as low as 0.1 μg/mL with high accuracy. In addition, a linear relationship was observed between the first canonical score and protein concentration, providing the potential for protein quantification using this sensor array. Furthermore, seven proteins spiked in artificial urine were successfully identified at 0.5 μg/mL with 100% discriminant accuracy. In comparison with previously reported protein sensor arrays, this TC-GUMBOS-based fluorescence sensor array provides favorable discriminant accuracy at a much lower protein concentration.[6d,e,7b,25,26] Thus, we believe that this TC-GUMBOS-based sensor array has great potential for highly sensitive and accurate medical diagnosis as well as for discrimination of other biomolecules.

MATERIALS AND METHODS

Reagents. Thiacarbocyanine (TC) dyes, 3,3′-diethylthiacyanine iodide ([TC0][I]), 3,3′-diethylthiacarbocyanine iodide ([TC1][I]), and 3,3′-diethylthiadicarbocyanine iodide ([TC2][I]) were purchased from Sigma Aldrich (St. Louis, MO). Lysozyme (Lys) from chicken egg white, human transferrin (Trans) (>98%), albumin from human serum (HSA) (approx. 99%), cytochrome c (Cyt-c), immunoglobulin G from human serum (IgG), fibrinogen from human plasma (Fib), human hemoglobin (Hb), ammonium persulfate, sodium phosphate dibasic, and sodium phosphate monobasic were all also purchased from Sigma Aldrich. Lithium bis(trifluoromethane)sulfonamide (Li[NTf2]) salt and lithium bis(pentafluoroethanesulfonyl)imide (Li[BETI]) salt were obtained from TCI Portland, Oregon. Artificial urine, HPLC-grade ethanol, and dichloromethane were acquired from VWR (Batavia, IL). Triple deionized ultrapure water (18.2 M Ω cm) was obtained using an Aries high-purity water system (West Berlin, NJ). All reagents were used as received without further purification.

Instrumentation. Ultraviolet−visible (UV−vis) absorption spectra were measured using a Shimadzu UV-3101PC UV−Vis scanning spectrometer (Shimadzu, Columbia, MD). Fluorescence emission spectra were recorded employing a Spex Fluorolog-3 spectrofluorimeter (model FL3-22TAU3; Jobin Yvon, Edison, NJ) with a slit width of 5 nm. All spectroscopic studies were performed using quartz cuvettes (Starna Cells).

Fourier transform infrared spectra (FT-IR) were collected through 128 scans in the 4000−650 cm^{-1} region with a resolution of 4 cm^{-1} in a Bruker Tensor 27 instrument (Billerica, MA) equipped with a PIKE MIRacle single-bounce attenuated total reflectance (ATR) cell. Electrospray ionization mass spectrometry (ESI-MS) was accomplished using an Agilent 6210 system in positive and negative mode. Transmission electron microscopy (TEM) images were obtained for characterization of size and morphology using a JEOL JEM-1400 transmission electron microscope (München, Germany).

Synthesis and Characterization of TC-GUMBOS and Aggregates. TC-GUMBOS were synthesized using a metathesis reaction between iodide salt of each dye and Li[NTf2] or Li[BETI] at a molar ratio of 1:1.1. Reactions were performed in a biphasic system of DCM and water while stirring for 24 h in a dark place at room temperature. The DCM layer was washed several times with DI water to remove the byproduct (LiI). DCM was then removed by rotary evaporation. Finally, GUMBOS were freeze-dried to remove residual water. Resultant TC-GUMBOS were characterized by ESI-MS and FT-IR spectroscopy.

TC-GUMBOS aggregates were prepared using a simple reprecipitation method.[27] Briefly, 50 μL of 0.5 mM ethanolic solution of each TC-GUMBOS was dropped into 5 mL of 10 mM sodium phosphate buffer (pH = 7.4) under a sonication bath for 3 min. The resulting aqueous solution was left to rest for 15 min. Finally, 5 μL of each solution was dropped into a TEM grid to characterize the aggregates.

Data Collection. Protein stock solutions of 200 μg/mL were prepared in 10 mM sodium phosphate buffer (pH = 7.4). Diluted solutions with concentrations ranging from 0.1 to 20 μg/mL were prepared from these stock solutions.

For sensing studies, 50 μL of 0.5 mM ethanolic TC-GUMBOS solution was dropped into 5 mL of protein solution and sonicated for 3 min. Then, the sensor−protein solution was allowed to stabilize for 15 min and absorption and fluorescence spectra were collected.

In this study, relative emission intensity change was employed as a sensor response (eq 1)

$$\text{relative emission intensity change} = \left(I/I_0 - 1\right) \quad (1)$$

Here, I and I_0 represent emission intensity of TC-GUMBOS in buffer with and without proteins, respectively. For each protein, six replicate samples were analyzed.

ASSOCIATED CONTENT

Supporting Information

The Supporting Information is available free of charge at https://pubs.acs.org/doi/10.1021/acssensors.0c00484.

Characterization and physicochemical properties of synthetized TC-GUMBOS, LDA plot obtained employing the reduced data, sensor responses and LDA plot at low concentrations of proteins, sensor responses at different protein concentrations, canonical plot obtained for each protein and the relationship between the first canonical and the protein concentration, and absorption and fluorescence spectra of each sensor in the presence of each protein (PDF)

AUTHOR INFORMATION

Corresponding Author

Isiah M. Warner − *Chemistry Department, Louisiana State University, Baton Rouge, Lousiana 70803, United States;* orcid.org/0000-0002-5336-7653; Phone: +1 225-578-2829; Email: iwarner@lsu.edu; Fax: +1 225-578-3971

Authors

Rocío L. Pérez − *Chemistry Department, Louisiana State University, Baton Rouge, Lousiana 70803, United States*

Mingyan Cong − *Chemistry Department, Louisiana State University, Baton Rouge, Lousiana 70803, United States*

Stephanie R. Vaughan − *Chemistry Department, Louisiana State University, Baton Rouge, Lousiana 70803, United States*

Caitlan E. Ayala − *Chemistry Department, Louisiana State University, Baton Rouge, Lousiana 70803, United States*

Waduge Indika S. Galpothdeniya − *Chemistry Department, Louisiana State University, Baton Rouge, Lousiana 70803, United States*

John K. Mathaga − *Chemistry Department, Louisiana State University, Baton Rouge, Lousiana 70803, United States*

Complete contact information is available at: https://pubs.acs.org/10.1021/acssensors.0c00484

Notes

The authors declare no competing financial interest.

https://dx.doi.org/10.1021/acssensors.0c00484
ACS Sens. 2020, 5, 2422−2429

■ ACKNOWLEDGMENTS

The authors gratefully acknowledge financial support through NASA cooperative agreement NNX 16AQ93A under contract number NASA/LEQSF (2016-19)-Phase 3-10 and the National Science Foundation under grant no. CHE-1905105. Any opinions, findings, and conclusions or recommendations expressed in this material are those of the author(s) and do not necessarily reflect the views of the National Science Foundation. The use of LSU Shared Instrumentation Facility is also acknowledged.

■ ABBREVIATIONS

[BETI]−, bis(pentafluoroethanesulfonyl)imide; Cyt-C, cytochrome-C; ELISA, enzyme-linked immunosorbent assay; ESI-MS, electrospray ionization mass spectroscopy; Fib, fibrinogen; FT-IR, Fourier transform infrared spectroscopy; GUMBOS, group of uniform materials based on organic salts; HSA, human serum albumin; Hb, hemoglobin; HPLC, high-pressure liquid chromatography; IgG, immunoglobulin G; I, emission intensity; I_0, initial emission intensity; LDA, linear discriminant analysis; Lys, lysosome; [NTf2]−, bis-(trifluoromethylsulfonyl)imide; pI, isoelectric points; PCA, principal component analysis; PD, polymethine dyes; TC, thiacarbocyanine dyes; [TC0]+, 3,3′-diethylthiacyanine cation; [TC1]+,, 3,3′-diethylthiacarbocyanine action; [TC2]+, 3,3′-diethylthiadicarbocyanine cation; TEM, transmission electron microscopy; Trans, transferrin

■ REFERENCES

(1) (a) Stoeva, S. I.; Lee, J.-S.; Smith, J. E.; Rosen, S. T.; Mirkin, C. A. Multiplexed Detection of Protein Cancer Markers with Biobarcoded Nanoparticle Probes. *J. Am. Chem. Soc.* **2006**, *128*, 8378−8379. (b) Kaushik, A.; Tiwari, S.; Dev Jayant, R.; Marty, A.; Nair, M. Towards detection and diagnosis of Ebola virus disease at point-of-care. *Biosens. Bioelectron.* **2016**, *75*, 254−272. (c) Kumar, V.; Brent, J. R.; Shorie, M.; Kaur, H.; Chadha, G.; Thomas, A. G.; Lewis, E. A.; Rooney, A. P.; Nguyen, L.; Zhong, X. L.; Burke, M. G.; Haigh, S. J.; Walton, A.; McNaughter, P. D.; Tedstone, A. A.; Savjani, N.; Muryn, C. A.; O'Brien, P.; Ganguli, A. K.; Lewis, D. J.; Sabherwal, P. Nanostructured Aptamer-Functionalized Black Phosphorus Sensing Platform for Label-Free Detection of Myoglobin, a Cardiovascular Disease Biomarker. *ACS Appl. Mater. Interfaces* **2016**, *8*, 22860−22868. (d) Xue, J.; Yang, L.; Jia, Y.; Wang, H.; Zhang, N.; Ren, X.; Ma, H.; Wei, Q.; Ju, H. Electrochemiluminescence Double Quenching System Based on Novel Emitter GdPO4:Eu with Low-Excited Positive Potential for Ultrasensitive Procalcitonin Detection. *ACS Sens.* **2019**, *4*, 2825−2831.

(2) (a) Hornbeck, P. Enzyme-linked immunosorbent assays. *Curr. Protoc. Immunol.* **1992**, *1*, 2.1.1−2.1.22. (b) Ambrosi, A.; Airò, F.; Merkoçi, A. Enhanced gold nanoparticle based ELISA for a breast cancer biomarker. *Anal. Chem.* **2010**, *82*, 1151−1156. (c) Ikeda, T. Protein A immunocapture assay detecting antibodies to fluke cysteine proteinases for immunodiagnosis of human paragonimiasis and fascioliasis. *J. Helminthol.* **2001**, *75*, 245−249.

(3) (a) Jia, C.-P.; Zhong, X.-Q.; Hua, B.; Liu, M.-Y.; Jing, F.-X.; Lou, X.-H.; Yao, S.-H.; Xiang, J.-Q.; Jin, Q.-H.; Zhao, J.-L. Nano-ELISA for highly sensitive protein detection. *Biosens. Bioelectron.* **2009**, *24*, 2836−2841. (b) Dille, B. J.; Surowy, T. K.; Gutierrez, R. A.; Coleman, P. F.; Knigge, M. F.; Carrick, R. J.; Aach, R. D.; Hollinger, F. B.; Stevens, C. E.; Barbosa, L. H.; Nemo, G. J.; Mosley, J. W.; Dawson, G. J.; Mushahwar, I. K. An ELISA for detection of antibodies to the E2 protein of GB virus C. *J. Infect. Dis.* **1997**, *175*, 458−461. (c) Butler, J. E. Enzyme-linked immunosorbent assay. *J. Immunoassay* **2000**, *21*, 165−209.

(4) (a) Kitamura, Y.; Usami, R.; Ichihara, S.; Kida, H.; Satoh, M.; Tomimoto, H.; Murata, M.; Oikawa, S. Plasma protein profiling for potential biomarkers in the early diagnosis of Alzheimer's disease. *Neurol. Res.* **2017**, *39*, 231−238. (b) Pagaduan, J. V.; Sahore, V.; Woolley, A. T. Applications of microfluidics and microchip electrophoresis for potential clinical biomarker analysis. *Anal. Bioanal. Chem.* **2015**, *407*, 6911−6922. (c) Davalieva, K.; Kiprijanovska, S.; Komina, S.; Petrusevska, G.; Zografska, N. C.; Polenakovic, M. Proteomics analysis of urine reveals acute phase response proteins as candidate diagnostic biomarkers for prostate cancer. *Proteome Sci.* **2015**, *13*, 2.

(5) (a) Zhang, R.; Wang, S.; Huang, X.; Yang, Y.; Fan, H.; Yang, F.; Li, J.; Dong, X.; Feng, S.; Anbu, P.; Gopinath, S. C. B.; Xin, T. Gold-nanourchin seeded single-walled carbon nanotube on voltammetry sensor for diagnosing neurogenerative Parkinson's disease. *Anal. Chim. Acta* **2020**, 142. (b) Yagati, A. K.; Pyun, J.-C.; Min, J.; Cho, S. Label-free and direct detection of C-reactive protein using reduced graphene oxide-nanoparticle hybrid impedimetric sensor. *Bioelectrochemistry* **2016**, *107*, 37−44.

(6) (a) De, M.; Rana, S.; Akpinar, H.; Miranda, O. R.; Arvizo, R. R.; Bunz, U. H.; Rotello, V. M. Sensing of proteins in human serum using conjugates of nanoparticles and green fluorescent protein. *Nat. Chem.* **2009**, *1*, 461−465. (b) Miranda, O. R.; You, C.-C.; Phillips, R.; Kim, I.-B.; Ghosh, P. S.; Bunz, U. H. F.; Rotello, V. M. Array-based sensing of proteins using conjugated polymers. *J. Am. Chem. Society* **2007**, *129*, 9856−9857. (c) Galpothdeniya, W. I. S.; Fronczek, F. R.; Cong, M.; Bhattarai, N.; Siraj, N.; Warner, I. M. Tunable GUMBOS-based sensor array for label-free detection and discrimination of proteins. *J. Mater. Chem. B* **2016**, *4*, 1414−1422. (d) Niamnont, N.; Mungkarndee, R.; Techakriengkrai, I.; Rashatasakhon, P.; Sukwattanasinitt, M. Protein discrimination by fluorescent sensor array constituted of variously charged dendritic phenylene−ethynylene fluorophores. *Biosens. Bioelectron.* **2010**, *26*, 863−867. (e) Kong, H.; Liu, D.; Zhang, S.; Zhang, X. Protein sensing and cell discrimination using a sensor array based on nanomaterial-assisted chemiluminescence. *Anal. Chem.* **2011**, *83*, 1867−1870. (f) Bunz, U. H. F.; Rotello, V. M. Gold nanoparticle−fluorophore complexes: sensitive and discerning "noses" for biosystems sensing. *Angew. Chem. Int. Ed.* **2010**, *49*, 3268−3279.

(7) (a) Saha, K.; Agasti, S. S.; Kim, C.; Li, X.; Rotello, V. M. Gold nanoparticles in chemical and biological sensing. *Chem. Rev.* **2012**, *112*, 2739−2779. (b) Wei, X.; Wang, Y.; Zhao, Y.; Chen, Z. Colorimetric sensor array for protein discrimination based on different DNA chain length-dependent gold nanoparticles aggregation. *Biosens. Bioelectron.* **2017**, *97*, 332−337. (c) Ramanathan, M.; Patil, M.; Epur, R.; Yun, Y.; Shanov, V.; Schulz, M.; Heineman, W. R.; Datta, M. K.; Kumta, P. N. Gold-coated carbon nanotube electrode arrays: Immunosensors for impedimetric detection of bone biomarkers. *Biosens. Bioelectron.* **2016**, *77*, 580−588.

(8) You, C.-C.; Miranda, O. R.; Gider, B.; Ghosh, P. S.; Kim, I.-B.; Erdogan, B.; Krovi, S. A.; Bunz, U. H. F.; Rotello, V. M. Detection and identification of proteins using nanoparticle−fluorescent polymer 'chemical nose' sensors. *Nat. Nanotechnol.* **2007**, *2*, 318.

(9) (a) Gooding, J. J.; Wibowo, R.; Liu; Yang, W.; Losic, D.; Orbons, S.; Mearns, F. J.; Shapter, J. G.; Hibbert, D. B. Protein electrochemistry using aligned carbon nanotube arrays. *J. Am. Chem. Soc* **2003**, *125*, 9006−9007. (b) Chen, R. J.; Choi, H. C.; Bangsaruntip, S.; Yenilmez, E.; Tang, X.; Wang, Q.; Chang, Y.-L.; Dai, H. An investigation of the mechanisms of electronic sensing of protein adsorption on carbon nanotube devices. *J. Am. Chem. Soc.* **2004**, *126*, 1563−1568. (c) Landry, M. P.; Ando, H.; Chen, A. Y.; Cao, J.; Kottadiel, V. I.; Chio, L.; Yang, D.; Dong, J.; Lu, T. K.; Strano, M. S. Single-molecule detection of protein efflux from microorganisms using fluorescent single-walled carbon nanotube sensor arrays. *Nat. Nanotechnol.* **2017**, *12*, 368.

(10) (a) Zhou, H.; Baldini, L.; Hong, J.; Wilson, A. J.; Hamilton, A. D. Pattern recognition of proteins based on an array of functionalized porphyrins. *J. Am. Chem. Soc.* **2006**, *128*, 2421−2425. (b) Kubota, R.; Hamachi, I. Protein recognition using synthetic small-molecular binders toward optical protein sensing in vitro and in live cells. *Chem. Soc. Rev.* **2015**, *44*, 4454−4471.

https://dx.doi.org/10.1021/acssensors.0c00484
ACS Sens. 2020, 5, 2422−2429

(11) (a) Tesfai, A.; El-Zahab, B.; Bwambok, D. K.; Baker, G. A.; Fakayode, S. O.; Lowry, M.; Warner, I. M. Controllable Formation of Ionic Liquid Micro- and Nanoparticles via a Melt−Emulsion−Quench Approach. *Nano Lett.* **2008**, *8*, 897−901. (b) Warner, I. M.; El-Zahab, B.; Siraj, N. Perspectives on Moving Ionic Liquid Chemistry into the Solid Phase. *Anal. Chem.* **2014**, *86*, 7184−7191.
(12) Kirstein, S.; Daehne, S. J-aggregates of amphiphilic cyanine dyes: Self-organization of artificial light harvesting complexes. *Int. J. Photoenergy* **2006**, *2006*, 1.
(13) Bricks, J. L.; Slominskii, Y. L.; Panas, I. D.; Demchenko, A. P. Fluorescent J-aggregates of cyanine dyes: basic research and applications review. *Methods appl. fluoresc.* **2018**, *6*, No. 012001.
(14) (a) Chowdhury, A.; Wachsmann-Hogiu, S.; Bangal, P. R.; Raheem, I.; Peteanu, L. A. Characterization of chiral H and J aggregates of cyanine dyes formed by DNA templating using stark and fluorescence spectroscopies. *J. Phys. Chem. B* **2001**, *105*, 12196−12201. (b) Hranisavljevic, J.; Dimitrijevic, N. M.; Wurtz, G. A.; Wiederrecht, G. P. Photoinduced charge separation reactions of J-aggregates coated on silver nanoparticles. *J. Am. Chem. Soc.* **2002**, *124*, 4536−4537. (c) Lim, I.-I. S.; Goroleski, F.; Mott, D.; Kariuki, N.; Ip, W.; Luo, J.; Zhong, C.-J. Adsorption of cyanine dyes on gold nanoparticles and formation of J-aggregates in the nanoparticle assembly. *J. Phys. Chem. B* **2006**, *110*, 6673−6682. (d) Peyratout, C.; Daehne, L. Aggregation of thiacyanine derivatives on polyelectrolytes. *Phys. Chem. Chem. Phys.* **2002**, *4*, 3032−3039. (e) Gadde, S.; Batchelor, E. K.; Kaifer, A. E. Controlling the Formation of Cyanine Dye H-and J-Aggregates with Cucurbituril Hosts in the Presence of Anionic Polyelectrolytes. *Chem. A Eu. J.* **2009**, *15*, 6025−6031. (f) Pal, S. K.; Datta, A.; Mandal, D.; Bhattacharyya, K. Photoisomerisation of diethyloxadicarbocyanine iodide in micelles. *Chem. Phys. Lett.* **1998**, *288*, 793−798. (g) Sabaté, R.; Gallardo, M.; de la Maza, A.; Estelrich, J. A spectroscopy study of the interaction of pinacyanol with n-dodecyltrimethylammonium bromide micelles. *Langmuir* **2001**, *17*, 6433−6437. (h) García-Jiménez, F.; Khramov, M. I.; Sánchez-Obregón, R.; Collera, O. Formation of J-aggregates of cyanine dyes in bilayer lipid vesicles. *Chem. Phys. Lett.* **2000**, *331*, 42−46. (i) Levitus, M.; Ranjit, S. Cyanine dyes in biophysical research: the photophysics of polymethine fluorescent dyes in biomolecular environments. *Q. Rev. Biophys.* **2011**, *44*, 123−151.
(15) (a) Tatikolov, A. S.; Costa, S. M. B. Complexation of polymethine dyes with human serum albumin: a spectroscopic study. *Biophys. Chem.* **2004**, *107*, 33−49. (b) Armitage, B. A. Cyanine dye−DNA interactions: intercalation, groove binding, and aggregation. In *DNA binders and related subjects*, Springer: 2005; pp 55−76.
(16) (a) McLachlan, G. *Discriminant analysis and statistical pattern recognition*. John Wiley & Sons: 2004; Vol. *544*; (b) Fisher, R. A. The use of multiple measurements in taxonomic problems. *Ann. Hum. Genet.* **1936**, *7*, 179−188.
(17) (a) Wang, H.; Wang, Z.; Leng, Y.; Wu, X.; Li, Q. PCA plus F-LDA: A new approach to face recognition. *Int J Pattern Recogn Artif. Intell.* **2011**, *21*, 1059−1068. (b) Yang, J.; Yang, J.-y. Why can LDA be performed in PCA transformed space? *Pattern Recognit.* **2003**, *36*, 563−566. (c) Belhumeur, P. N.; Hespanha, J. P.; Kriegman, D. J. Eigenfaces vs. fisherfaces: Recognition using class specific linear projection. *IEEE Trans. Pattern Anal Mach. Int.* **1997**, *19*, 711−720. (d) Yu, H.; Yang, J. A direct LDA algorithm for high-dimensional data—with application to face recognition. *Pattern Recognit.* **2001**, *34*, 2067−2070.
(18) (a) Khairutdinov, R. F.; Serpone, N. Photophysics of cyanine dyes: Subnanosecond relaxation dynamics in monomers, dimers, and H-and J-aggregates in solution. *J. Phys. Chem. B* **1997**, *101*, 2602−2610. (b) Gieseking, R. L.; Mukhopadhyay, S.; Risko, C.; Marder, S. R.; Brédas, J. L. 25th Anniversary Article: Design of Polymethine Dyes for All-Optical Switching Applications: Guidance from Theoretical and Computational Studies. *Adv. Mater.* **2014**, *26*, 68−84.
(19) (a) Tatikolov, A. S. Polymethine dyes as spectral-fluorescent probes for biomacromolecules. *J. Photochem. Photobiol., C* **2012**, *13*, 55−90. (b) Strekowski, L. *Heterocyclic polymethine dyes: synthesis, properties and applications*. Springer: 2008; Vol. *14*; (c) Nordén, B.; Tjerneld, F. Optical studies on complexes between DNA and pseudoisocyanine. *Biophys. Chem.* **1976**, *6*, 31−45. (d) Cao, R.; Venezia, C. F.; Armitage, B. A. Investigation of DNA binding modes for a symmetrical cyanine dye trication: effect of DNA sequence and structure. *J. Biomol. Struct. Dyn.* **2001**, *18*, 844−857. (e) Yarmoluk, S. M.; Lukashov, S. S.; Losytskyy, M. Y.; Akerman, B.; Kornyushyna, O. S. Interaction of cyanine dyes with nucleic acids: XXVI. Intercalation of the trimethine cyanine dye Cyan 2 into double-stranded DNA: study by spectral luminescence methods. *Spectrochim. Acta, Part A* **2002**, *58*, 3223−3232.
(20) (a) Chen, S. Y.; Horng, M. L.; Quitevis, E. L. Picosecond spectroscopic studies of electronic energy relaxation in H-aggregates of 1, 1′-diethyl-2, 2′-dicarbocyanine on colloidal silica. *J. Phys. Chem.* **1989**, *93*, 3683−3688. (b) West, W.; Pearce, S. The dimeric state of cyanine dyes. *J. Phys. Chem.* **1965**, *69*, 1894−1903.
(21) (a) Volkova, K. D.; Kovalska, V. B.; Balanda, A. O.; Losytskyy, M. Y.; Golub, A. G.; Vermeij, R. J.; Subramaniam, V.; Tolmachev, O. I.; Yarmoluk, S. M. Specific fluorescent detection of fibrillar α-synuclein using mono- and trimethine cyanine dyes. *Bioorg. Med. Chem* **2008**, *16*, 1452−1459. (b) Kuzmin, V. A.; Nekipelova, T. D.; Podrugina, T. A.; Golovina, G. V.; Kostyukov, A. A.; Temnov, V. V.; Doroshenko, I. A.; Radchenko, E. V.; Palyulin, V. A.; Zefirov, N. S. Complex formation of albumin with tricarbocyanine dyes containing phosphonate groups. *Photochem. Photobiol. Sci.* **2016**, *15*, 1377−1384.
(22) Yao, H.; Ashiba, K. Highly fluorescent organic nanoparticles of thiacyanine dye: A synergetic effect of intermolecular H-aggregation and restricted intramolecular rotation. *RSC Adv.* **2011**, *1*, 834−838.
(23) Das, S.; Bwambok, D.; El-Zahab, B.; Monk, J.; de Rooy, S. L.; Challa, S.; Li, M.; Hung, F. R.; Baker, G. A.; Warner, I. M. Nontemplated Approach to Tuning the Spectral Properties of Cyanine-Based Fluorescent NanoGUMBOS. *Langmuir* **2010**, *26*, 12867−12876.
(24) (a) Chibisov, A. K.; Görner, H. Photophysics of aggregated 9-methylthiacarbocyanine bound to polyanions. *Chem. Phys. Lett.* **2002**, *357*, 434−439. (b) Mamchits, E. G.; Nasimova, I. R.; Makhaeva, E. E.; Khokhlov, A. R. Effect of polyelectrolytes on aggregation of a cyanine dye. *Polymer Science Series A* **2006**, *48*, 91−96.
(25) Xu, S.; Su, Z.; Zhang, Z.; Nie, Y.; Wang, J.; Ge, G.; Luo, X. Rapid synthesis of nitrogen doped carbon dots and their application as a label free sensor array for simultaneous discrimination of multiple proteins. *J. Mater. Chem. B* **2017**, *5* (44), 8748−8753.
(26) Xu, S.; Lu, X.; Yao, C.; Huang, F.; Jiang, H.; Hua, W.; Na, N.; Liu, H.; Ouyang, J. A Visual Sensor Array for Pattern Recognition Analysis of Proteins Using Novel Blue-Emitting Fluorescent Gold Nanoclusters. *Anal. Chem.* **2014**, *86* (23), 11634−11639.
(27) (a) Cong, M.; Siraj, N.; Bhattarai, N.; Kolic, P. E.; McCarter, K. S.; Chhotaray, P. K.; Warner, I. M. Ratiometric fluorescence detection of hydroxyl radical using cyanine-based binary nanoGUMBOS. *Sens. Actuators, B* **2018**, *257*, 993−1000. (b) Siraj, N.; el-Zahab, B.; Hamdan, S.; Karam, T. E.; Haber, L. H.; Li, M.; Fakayode, S. O.; Das, S.; Valle, B.; Strongin, R. M.; Patonay, G.; Sintim, H. O.; Baker, G. A.; Powe, A.; Lowry, M.; Karoli, J. O.; Geddes, C. D.; Warner, I. M. Fluorescence, phosphorescence, and chemiluminescence. *Anal. Chem* **2015**, *88*, 170−202.

https://dx.doi.org/10.1021/acssensors.0c00484
ACS Sens. 2020, 5, 2422−2429